Proceedings of the 8th International Conference on Civil Engineering for Sustainable Development (ICCESD 2026), 5~7 February 2026, KUET, Khulna, Bangladesh

EFFECTS OF TIME-DEPENDENT THREE-DIMENSIONAL BEHAVIOR ON ANCHORED DIAPHRAGM WALL SUPPORT SYSTEM IN CLAYEY SOIL

Mahendra Patel[1*] and Baleshwar Singh[2]

[1] *Research scholar, Department of Civil Engineering, Indian Institute of Technology Guwahati, Assam, India, e-mail: mpatel@iitg.ac.in*
[2] *Professor, Department of Civil Engineering, Indian Institute of Technology Guwahati, Assam, India, e-mail: baleshwar@iitg.ac.in*

***Corresponding Author**

ABSTRACT

Large urban excavations require efficient utilization of underground space but pose considerable challenges in clayey soils due to their time-dependent behavior, which influences the performance of supporting systems. Such behavior influences not only the lateral displacement of retaining walls but also the movement of the retained soil, potentially affecting adjacent structures. The generation of negative excess pore water pressure further complicates the analysis and design process. Conventional two-dimensional simulations often neglect critical three-dimensional effects such as anchor spacing, wall length and load distribution, that affect the stress and displacement responses of the excavation system. To address these limitations, this study investigates the behavior of a 15 m deep and 30 m wide excavation supported by a three-level anchored diaphragm wall in clayey soil, emphasizing the influence of three-dimensional interactions and time-dependent effects on excavation performance. A three-dimensional finite element model has been developed using PLAXIS 3D software to simulate realistic field conditions of a deep excavation. The model has been validated against field-monitored data from a case study, demonstrating good agreement with observed responses. The Hardening Soil model with small-strain stiffness has been adopted to capture the interaction between the diaphragm wall and surrounding soil. Construction activities, including dewatering, excavation, and the sequential installation and pre-stressing of anchors, have been simulated in a staged manner with explicit consideration of construction time. Based on an excavation rate of 0.1 m/day and 32 days allocated for anchoring and prestressing, the total construction duration has reached to 246 days. Post-excavation performance has been further analyzed for a period of 84 months (7 years) following the final excavation stage. A comprehensive parametric study has been conducted to systematically investigate the influence of two key variables: excavation geometry and soil permeability. The objective is to highlight the effects of time-dependent consolidation on lateral wall displacement, development of bottom heave, and pore water pressure dissipation, during and after excavation. The responses are presented in the form of graphs for the period of during excavation and post-excavation. The results reveal that the diaphragm wall and the adjacent soil undergo deep inward movement during excavation. Maximum bottom heave occurs at the centre of the excavation, while a zone of negative excess pore water pressure develops at a certain depth below the excavation level. Wall displacement decreases with smaller L/B ratios, with post-excavation variations becoming negligible across all cases. Smaller L/B ratios result in greater bottom heave during the post-excavation stage. Soils with higher permeability generate lower excess pore pressures during excavation but exhibit slower dissipation in the post-excavation stage. Although wall displacement stabilizes after final excavation, bottom heave continues to increase with increasing soil permeability. The final steady-state pore pressures are found to be less negative in soils with higher permeability and in cases with smaller L/B ratios.

Keywords: *Excavation support system, Three-dimensional analysis, Long-term performance, Numerical modelling*

1. INTRODUCTION

Deep excavations are a crucial component of modern urban infrastructure projects, enabling the construction of underground facilities such as basements, subways, and parking structures in densely built environments. With the continuous expansion of metropolitan areas and the scarcity of surface space, underground construction has become a viable solution to meet space and functional requirements. These projects, however, induce significant changes in the stress and displacement fields of surrounding soils, posing risks to adjacent structures and existing utilities (Clough & O'Rourke, 1990; Long, 2001). Therefore, the design and analysis of reliable support systems play a crucial role in ensuring both stability and serviceability during excavation (Ou, 2006). Conventional two-dimensional (2D) analyses, although widely used, often idealise the problem assuming plane strain conditions, which may overlook critical three-dimensional (3D) effects arising from non-uniform excavation geometry, corner interaction, spatial anchor distribution, and sequential excavation processes (Finno & Roboski, 2005; Hsiung et al., 2018). These 3D effects can substantially influence wall displacements, bending moments, and the mobilization of anchor forces. Hence, 3D numerical analyses are essential for realistically capturing the complex soil-structure interaction mechanism and achieving more accurate predictions of ground responses.

Furthermore, the behavior of clayey soil is inherently time-dependent, where consolidation governs stress redistribution and deformation over time (Harahap & Ou, 2020). Post-excavation consolidation may cause progressive ground settlement, changes in anchor forces and delayed wall displacement, which cannot be captured in undrained analyses. Considering time-dependent effects, such as consolidation, is therefore crucial to evaluate the long-term performance and safety of deep excavation systems, ensuring that both short-term stability and long-term deformation criteria are satisfied. The influence of excavation geometry, including length, width, and depth (Finno et al., 2007), as well as the surrounding soil conditions (Lu et al., 2023), can significantly impact the mechanical response of the system. These factors govern the spatial extent of deformation, pore water pressure dissipation and the resulting consolidation process. Ignoring these long-term effects can lead to inaccurate predictions of wall displacements, pore-water pressure, and bottom heave, which can evolve significantly after construction. Therefore, this study aims to address these challenges by integrating three-dimensional numerical modelling with time-dependent analysis to comprehensively evaluate the effects of excavation length and soil permeability on excavation responses, such as maximum lateral wall displacement, maximum bottom heave and pore-water pressure generation and dissipation.

2. FINITE ELEMENT MODEL

2.1 Soil Constitutive Model

The Hardening Soil with small-strain stiffness (HS-small) model is utilized in this study to simulate soil behavior. This model is an extension of the original HS model formulated by Schanz et al. (1999). It incorporates frictional hardening to describe plastic shear strain under deviatoric loading and cap hardening to account for plastic volumetric strain during primary compression, while failure is governed by the Mohr-Coulomb criterion. For simulation of unloading and reloading behavior, the model employs three reference stiffness parameters: (1) triaxial stiffness (E_{50}^{ref}), (2) triaxial unloading/reloading stiffness (E_{ur}^{ref}), and (3) oedometer loading stiffness (E_{oed}^{ref}). The primary input parameters for the model include E_{50}^{ref} at the reference confining pressure (p_{ref}), the power (m) in the stress-dependency formulation of stiffness, effective friction angle (ϕ), cohesion (c), failure ratio (R_f), and the unloading/reloading Poisson's ratio (ν_{ur}). The HS-small model introduces two additional parameters: the reference small-strain shear modulus (G_0^{ref}) and the shear strain ($\gamma_{0.7}$), defined as the strain level at which the secant shear modulus equals 0.7 times G_0^{ref}. In this study, the E_{ur}^{ref} and E_{oed}^{ref} are taken as 3.0 and 0.7 times the E_{50}^{ref}, respectively, following Calvello & Finno (2004).

2.2 Structural Model and Input Properties

An anchored wall support system consists of a diaphragm wall in combination with ground anchors. The diaphragm wall is modelled using a six-noded triangular elastic plate element. This element provides six degrees of freedom at each node. Ground anchors are modelled using a node-to-node anchor for the unbonded length and an embedded beam element for the bonded length. An embedded beam element is composed of beam elements equipped with specialized interface elements that facilitate interaction between the beam and the surrounding soil. The beam elements are three-noded line elements, each possessing six degrees of freedom. For soil-wall interaction, a 12-node interface element with a factor (R_{inter}) of 1 is used. These interface elements consist of node pairs compatible with the six-node triangular sides of soil or plate elements. The elastic plate elements are characterised by their stiffness properties (E, G and v). The node-to-node anchor's elastic behavior is defined by its axial stiffness (EA), while the embedded beam row is described by both its stiffness property (EA) and its interaction with the surrounding soil, represented by the skin friction parameter (T_{skin}). In this study, the diaphragm wall stiffness is reduced by 30% to account for bending-induced cracking in the concrete (Ou, 2006). The elastic modulus of the steel strands is taken as 210 GPa (Sabatini et al., 1999), while the stiffness of the anchor bar is reduced by 40%. The bonded length, modelled as a composite steel/grout section, incorporates a grout modulus reduced by 40% to consider grout cracking effects (Briaud & Lim, 1999). The grout diameter (D) is assumed equal to the anchor underreamed diameter for modelling simplicity. Table 1 summarizes the reduced support system input parameters used in the analysis.

Table 1: Support system properties used in the present study

Element	Parameter	Values
Diaphragm wall	Young's Modulus, E_w (MN/m^2)	17.36 x 10^3
	Shear Modulus, G_w (MN/m^2)	7.23 x 10^3
	Poission's ratio, v	0.20
Node-to-node anchor	Axial stiffness, EA (MN)	158.760
Embedded beam	Diameter, D (m)	0.55
	$T_{skin,\ start,\ max}$ (kN/m)	195.4
	$T_{skin,\ end,\ max}$ (kN/m)	195.4

2.3 Finite Element Mesh and Boundary Conditions

Three-dimensional finite element analyses were conducted using PLAXIS 3D software (Brinkgreve et al., 2015). The soil domain was discretized using 10-noded tetrahedral elements, with each node possessing three translational degrees of freedom. A domain analysis established sufficient lateral extents to prevent boundary effects for a 15 m deep and 30 m wide excavation supported by a diaphragm wall with three levels of anchors. Following this, a mesh convergence study was conducted using various mesh sizes, ultimately selecting a fine mesh for optimal accuracy. Exploiting the symmetry of the excavation geometry, a quarter model has been utilized to balance between computational efficiency and precision. The final base model, depicted in Figure 1, comprises 85,552 elements and 1,25,408 nodes, with an average element size of 3.359 m. In the figure, H_e denotes the maximum excavation depth, $B/2$ represents half of the excavation width, and $L/2$ represents half of the excavation length. The lateral domain extends to a distance equal to ten times the excavation depth from the wall to minimize boundary effects. The analysis incorporates a constant surcharge load (q) of 10 kPa applied over a width of 15 m, commencing 3 m from the diaphragm wall and applied around all sides of the excavation. The boundary conditions were defined as follows: no displacement allowed at the model base using pinned supports, only vertical displacement was permitted at the lateral boundaries with roller supports, and the top surface was free to displace in all directions. The left and front boundary serve as a closed seepage boundary (symmetry axes), whereas the right and back boundary function as an open seepage boundary.

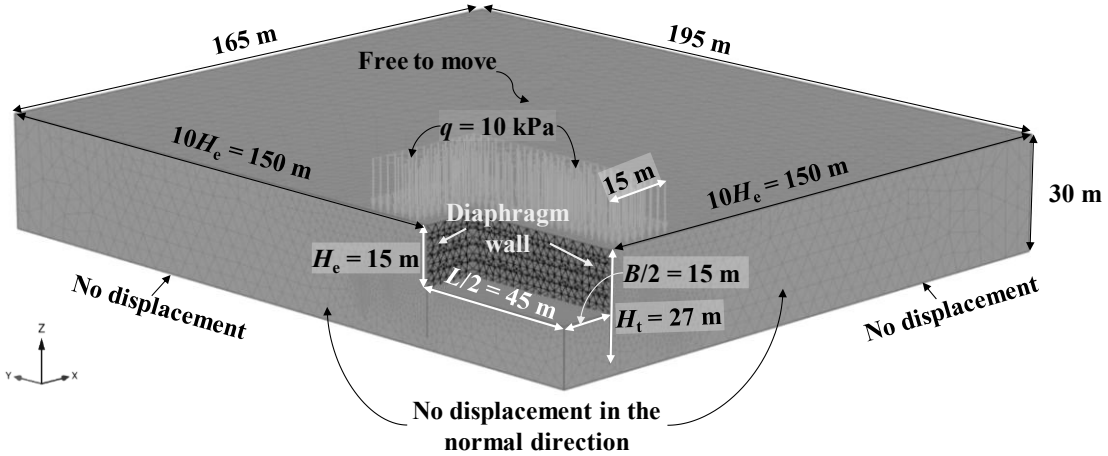

Figure 1: Typical one-quarter finite element model used for the analysis

2.4 Model Validation

The time-dependent numerical analysis was validated against a field study reported by Sills et al. (1978) for the Neasden underpass project in North London, which was monitored at different construction stages during and after excavation. The excavation, 8.6 m deep and 20 m wide, was supported by a 0.6 m thick diaphragm wall with four rows of pre-stressed anchors. These anchors were inclined at 40° and spaced at 4.57 m. The subsurface profile consists of stiff London clay extending to approximately 30 m depth. The HS-small soil parameters used for model validation, summarized in Table 2, were adopted from Hejazi et al. (2008).

Table 2: Soil parameters used in the present study

Parameter	London clay
Unit weight, γ (kN/m^3)	19.5
Cohesion, c (kPa)	7
Friction angle, ϕ (degrees)	20.5
Dilation angle, ψ (degrees)	4.81
Poisson's ratio, ν'	0.28
Ref. secant stiffness, E_{50}^{ref} (MPa)	32.5
Ref. oedometer stiffness, E_{oed}^{ref} (MPa)	22.75
Ref. unloading-reloading stiffness, E_{ur}^{ref} (MPa)	97.5
Ref. shear modulus, G_0^{ref} (MPa)	65
Stress dependency power, m	0.5
Threshold shear strain, $\gamma_{0.7}$	10^{-4}

The height of the diaphragm wall was 13 m. Its material properties are as follows: unit weight (γ_c) = 24 kN/m^3, Young's modulus (E) = 30 GPa, and Poisson's ratio (ν) = 0.2. All anchors were of the underreamed type, each having a 175 mm shaft diameter, a 535 mm underream diameter, and an underream spacing of 1150 mm. The anchors were prestressed to 460 kN, with an equivalent stiffness of 50 MN/m per anchor. The 3D plane strain model adopted for validation is illustrated in Figure 2. The computed lateral wall displacement profile and pore-water pressure at different construction stages (during and after final excavation) were compared with corresponding field measurements. Wall displacements were monitored using inclinometers installed in the wall, while pore-water pressures were measured by piezometers installed at various depths behind the wall. It was observed that the best agreement between the computed and measured results was achieved by adopting a coefficient of permeability (k) of 0.7×10^{-8} cm/s.

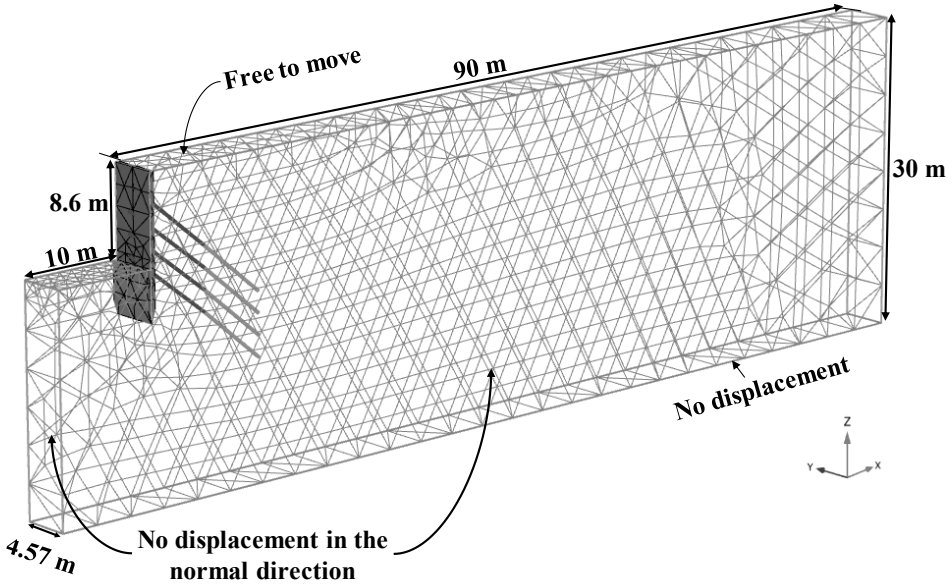

Figure 2: 3D plane strain model used for the validation

Figure 3 presents a comparison of the lateral wall displacement profiles recorded immediately after the final excavation and at 3 months post-excavation. The results indicate that the simulated wall response demonstrates a time-dependent pattern consistent with the field observations from inclinometer data. Moreover, the numerical predictions exhibit good agreement with the corresponding measured values.

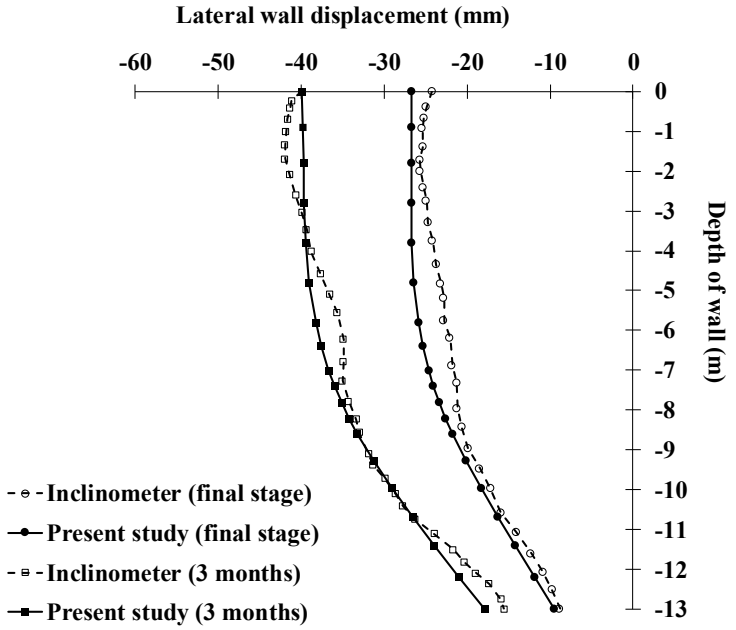

Figure 3: Comparison of lateral wall displacement profiles at different construction stages

Figure 4a and 4b present a comparison between the numerically predicted and measured pore-water pressure head profiles immediately following the final excavation and at 8 months post-excavation, respectively. The results show a reduction in pore-water pressure following the commencement of excavation, with the computed results demonstrating reasonable agreement with the field measurements. Overall, the numerical predictions correspond well with the measured data, thereby validating the accuracy of the numerical model.

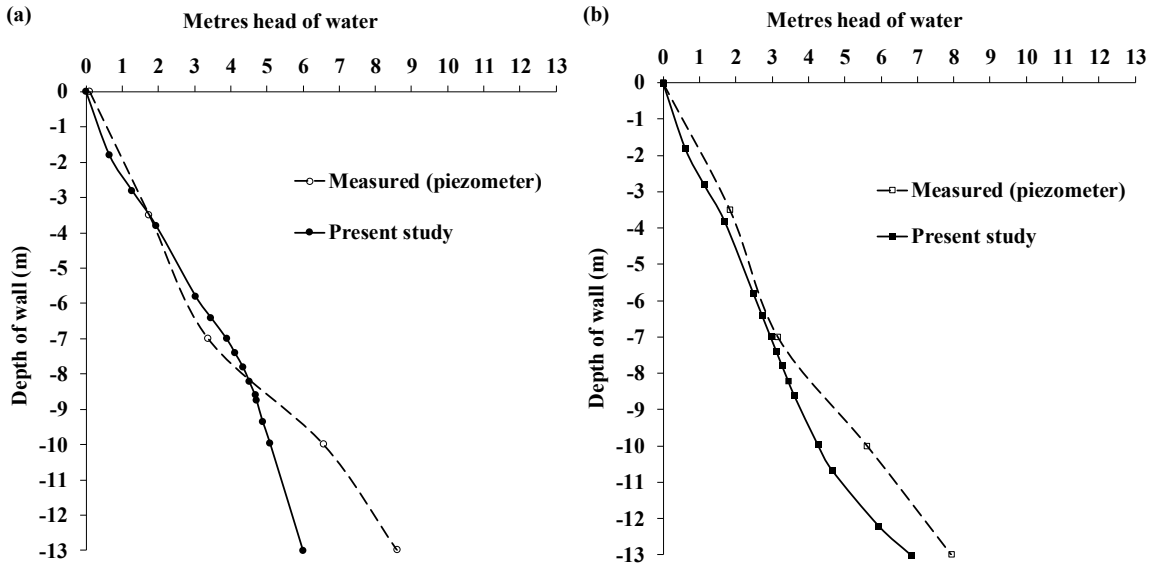

Figure 4: Comparison of pore water pressure head profile: (a) after the final excavation stage; (b) at 8 months post-excavation

2.5 Parametric Study

The present study investigates a base model involving an excavation measuring 15 m in depth, 30 m in width, and 90 m in length within the same stiff London clay (Table 2). The excavation is supported by a 0.9 m thick peripheral diaphragm wall with three levels of anchors. The first, second, and third anchors are installed at depths of 3 m, 7 m, and 11 m below the ground surface, respectively, having unbonded lengths of 16.30 m, 14.10 m, and 11.90 m. The other relevant design parameters are summarized in Table 3.

Table 3: Geometrical parameters used in the present study

Parameter	Notation	Geometrical properties
Excavation length (m)	L	90*, 60, 30
Excavation width (m)	B	30
Excavation depth (m)	H_e	15
Total wall depth to excavation depth ratio	H_t/H_e	1.80
Wall thickness (m)	t_w	0.9
Anchor inclination (°)	α	35°
Anchor prestress force (kN)	F_p	1400
Vertical anchor spacing (m)	S_v	4
Horizontal anchor spacing (m)	S_h	2.5
Anchor bonded length (m)	L_b	11

*Standard value if not varied

The excavation process has been simulated following these sequential steps:

1. Application of surcharge load.
2. Installation of the diaphragm wall using wished-in-place approach.
3. Excavation and dewatering: Excavation progresses to 0.5 m below each anchor level. Dewatering is performed by lowering the water level to excavation depth at each step while maintaining a constant water level at the ground surface on the retained side.
4. Installation and prestressing of anchors: After excavation at each stage, anchors are installed and prestressed at the specified depths.
5. Construction of base slab: Upon reaching the final excavation depth of 15 m, a base slab is constructed.

Steps 3 and 4 are repeated until the final excavation depth is achieved.

In this study, undrained and consolidation analyses are employed. The undrained analysis assumes that excess pore-water pressure generated by excavation does not dissipate, while the consolidation analysis captures the generation and dissipation of excess pore-water pressure over time. During the modelling process, steps 1 and 2 utilize undrained analysis, whereas steps 3, 4 and 5 incorporate consolidation effects. Post-construction analysis is conducted considering consolidation without any additional loading. An excavation rate of 0.1 m/day is adopted, and the soil permeability for the base case is taken as 0.7×10^{-8} cm/s (k_0). It is assumed that anchor installation at each level requires 32 days. Parametric analyses were conducted in two distinct series. In the first series, the excavation length has been varied to 30 m, 60 m and 90 m, corresponding to L/B ratios of 1, 2 and 3, respectively. The second series investigated the effect of increasing soil permeability to 10 (k_{10}) and 20 (k_{20}) times the value used in the base case (k_0). These parametric studies focused on quantifying the variations in key responses: (1) maximum lateral wall displacement (u_{max}), (2) maximum bottom heave ($u_{z,\,max}$) and (3) pore-water pressure. The time-dependent behavior of the excavation is evaluated over the entire period, encompassing the main excavation stages and the post-excavation consolidation period. The post-excavation performance has been analysed for a total duration of 84 months with time intervals selected to capture the progressive development of pressure acting within the system. Specifically, observations were taken at monthly intervals from 0 to 6 months, at three-month intervals from 6 to 24 months, and at six-month intervals from 24 to 84 months.

3. RESULTS AND DISCUSSION

3.1 Effects of Varying Excavation Length (L)

The increase in excavation length results in a progressive rise in maximum wall displacement (u_{max}) with time, as illustrated in Figure 5.

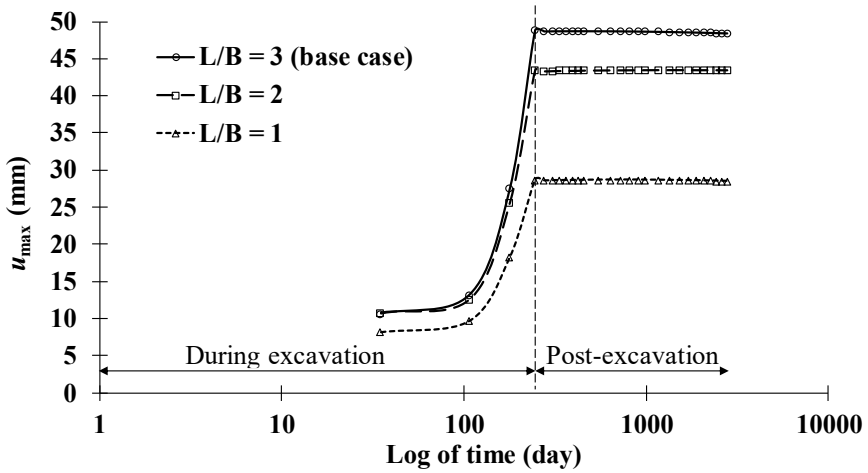

Figure 5: Effect of excavation length on maximum lateral wall displacement (u_{max})

During the excavation period, the displacement values for L/B ratios of 3 and 2 remain relatively close until the third excavation stage, while the displacement for L/B = 1 exhibits comparatively lower values throughout the entire excavation period. This behavior can be attributed to the enhanced corner stiffness effect associated with shorter excavation length. At the later stages of excavation, due to deep inward wall movement, the u_{max} occurred near the final excavation level. The u_{max} values at the final excavation stage for L/B ratios of 3, 2, and 1 are 48.45 mm, 43.51 mm, and 28.5 mm, respectively. Furthermore, the variation in displacement among all three cases during the post-excavation period appears insignificant, which may be attributed to the casting of the base slab.

The analysis indicates that the maximum bottom heave occurred at the node located at the centre of the excavation (0, 0, -15), which was therefore selected for comparison. As illustrated in Figure 6, a

progressive increase in the bottom heave is evident during and after the construction stages. During the excavation phase, all three cases exhibit identical heave behavior; however, post-excavation, the heave increases by 6.37 mm, 7.23 mm, and 10.14 mm for L/B ratios of 3, 2, and 1, respectively. These results demonstrate that a lower L/B ratio leads to greater bottom heave after excavation due to reduced lateral confinement.

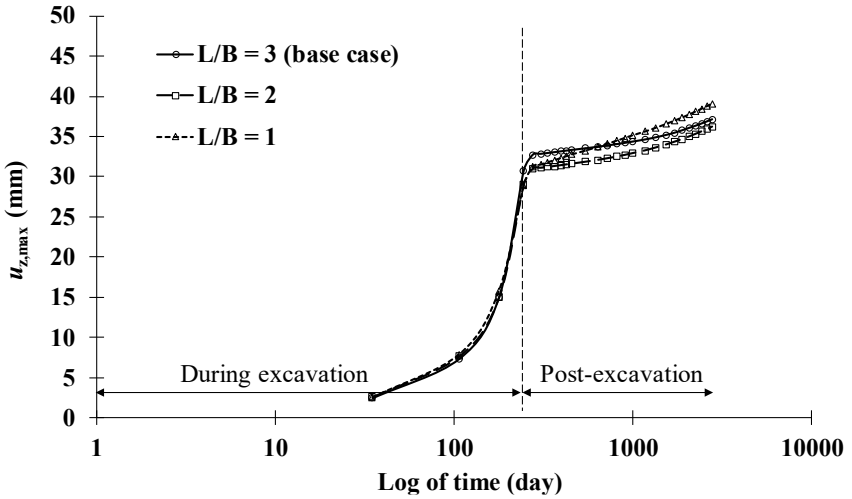

Figure 6: Effect of excavation length on maximum bottom heave ($u_{z,max}$)

The analysis shows the formation of a negative excess pore-water pressure zone at a depth of 5 m below the final excavation level. Accordingly, stress points located at (0.39, 0.38, -20.59), (0.215, 0.786, -20.268), and (0.53, 0.20, -20.37) corresponding to L/B ratios of 3, 2 and 1, respectively, are considered for comparative evaluation. Figure 7 illustrates the progressive development and subsequent dissipation of p_{excess} during the excavation and post-excavation stages, respectively.

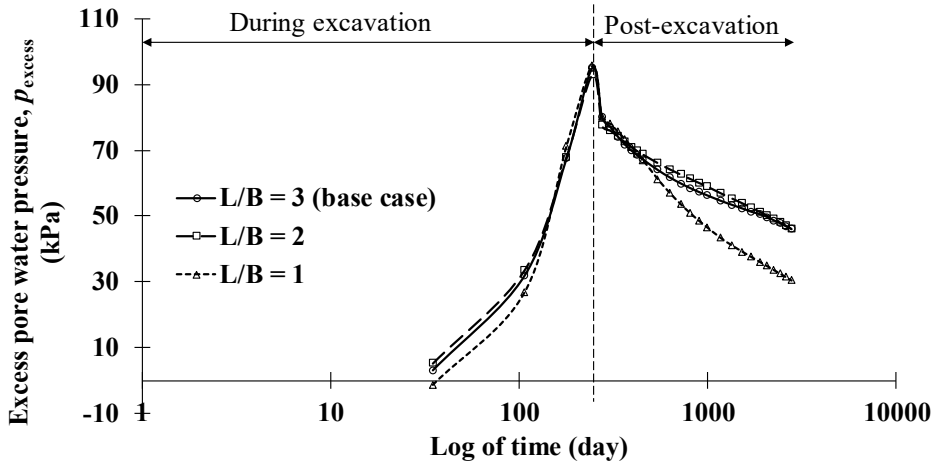

Figure 7: Effect of excavation length on excess pore-water pressure (p_{excess})

The p_{excess} profiles corresponding to L/B ratios of 3 and 2 exhibit similar trends, whereas the response for L/B = 1 demonstrates relatively lower p_{excess} throughout both stages. The active pore-water pressure state (p_{water}) is also assessed by evaluating stress points near the maximum wall displacement depth located behind the wall, as demonstrated in Figure 8. As shown, the stress state in all three cases decreases with a nearly uniform trend and similar values throughout the excavation stage, primarily due to stress release induced by excavation. The post-excavation behavior differs across all cases, with the lower L/B ratio showing greater increases in compressive stresses. This is likely due to more significant dissipation of excess pore-water pressure of tensile nature.

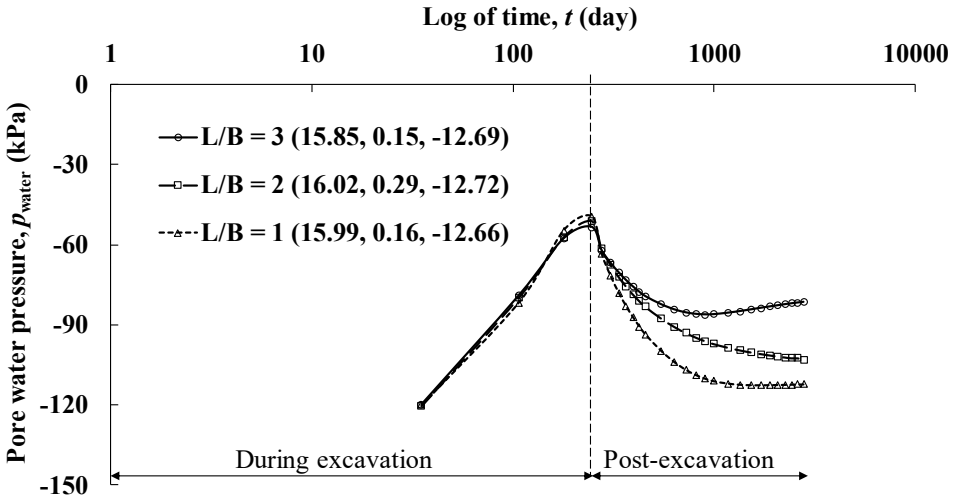

Figure 8: Effect of excavation length on active pore-water pressure (p_{water})

3.2 Effects of Varying Soil Permeability (k)

Figure 9 presents the effect of increasing soil permeability on maximum wall displacement (u_{max}) over time. The results indicate that u_{max} for all three cases remains nearly identical up to the third excavation stage. At the final excavation stage, the u_{max} values for cases k_0, k_{10} and k_{20} are 48.86 mm, 56.92 mm and 62.66 mm, respectively, highlighting the progressive influence of permeability on wall displacement. Following the final excavation stage, the wall displacement remains constant at the respective final values for all cases, primarily due to the casting of the base slab immediately after the final excavation stage.

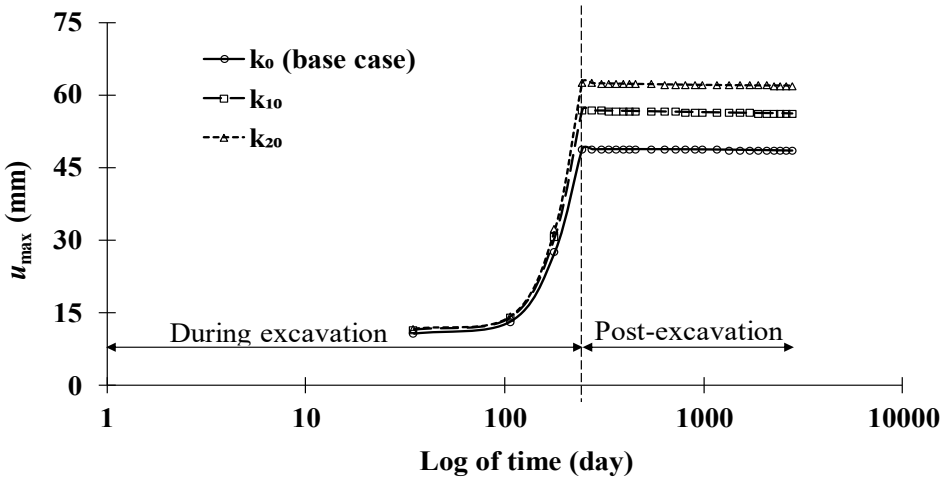

Figure 9: Effect of soil permeability on maximum lateral wall displacement (u_{max})

Figure 10 illustrates the effect of increasing soil permeability on the maximum bottom heave ($u_{z,max}$) over time at the centre of excavation (0, 0, -15). The results indicate a progressive increase in bottom heave with higher soil permeability after the second excavation stage. At the final excavation stage, the $u_{z,max}$ values for cases k_0, k_{10} and k_{20} are 30.73 mm, 39.74 mm and 47 mm, respectively. During the post-excavation stage, the $u_{z,max}$ further increases by 6.37 mm, 18.60 mm and 18.77 mm for cases k_0, k_{10} and k_{20}, respectively.

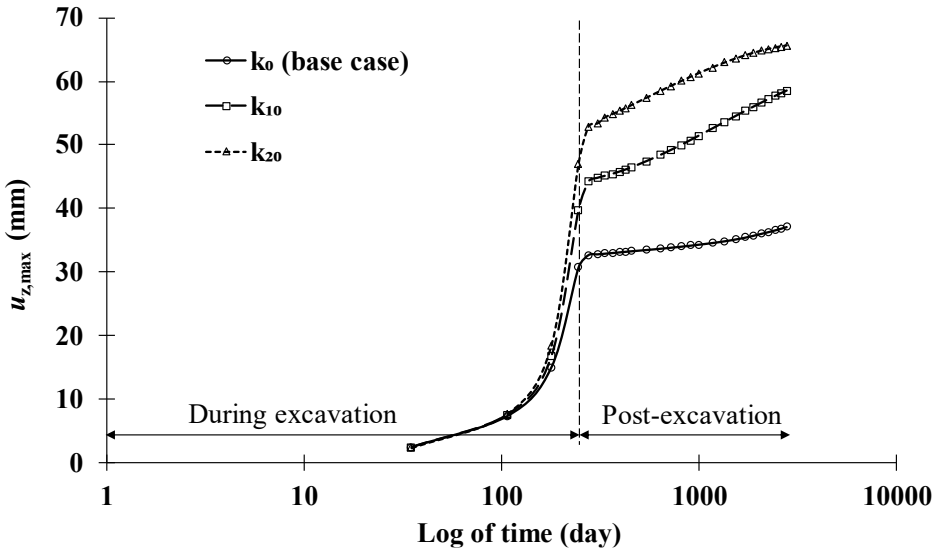

Figure 10: Effect of soil permeability on maximum bottom heave ($u_{z,max}$)

Figure 11 illustrates the variation of p_{excess} with increasing soil permeability at stress points (0.39, 0.38, -20.59), (0.215, 0.786, -20.268), and (0.53, 0.20, -20.37) corresponding to k_0, k_{10} and k_{20}, respectively. The results indicate that the soil with higher permeability exhibits reduced development of p_{excess}. A pronounced drop in p_{excess} is observed during the slab casting stage across all cases, which corresponds to the rapid dissipation of pore water pressure due to loading and water expulsion. Subsequently, a gradual reduction in p_{excess} with time is evident across all cases, indicating a consolidation process. The reductions in p_{excess} for cases k_0, k_{10} and k_{20} are approximately 34.046 kPa, 31.825 kPa and 23.412 kPa, respectively. The case with higher permeability exhibits a smaller reduction in p_{excess}, as a portion of the pressure has already dissipated more quickly.

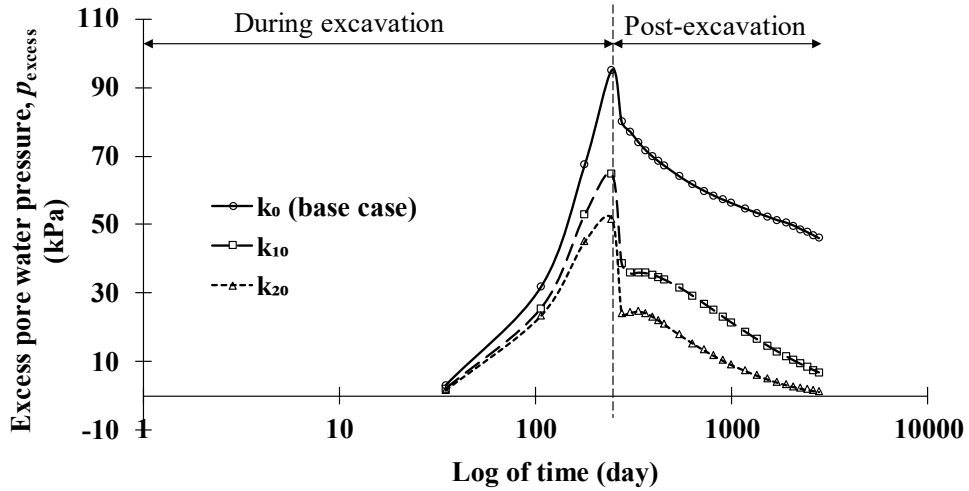

Figure 11: Effect of soil permeability on excess pore-water pressure (p_{excess})

Figure 12 illustrates the temporal variation of active pore-water pressure (p_{water}) with increasing soil permeability at stress points located at two depths just beyond the wall near the centre section. During the excavation period, all cases exhibit a gradual decrease in p_{water}, reflecting the rapid development of negative excess pore pressure in response to soil unloading. Soils with higher permeability (k_{10} and k_{20}) follow similar trends but show a smaller overall decrease compared to the base case, k_0 (Figure 12a), as higher permeability enables more rapid dissipation of negative p_{excess}. This behavior reverses at stress points located at greater depths (Figure 12b), which may be attributed to the effect of soil arching. Over an extended time, pore pressure stabilizes, and the final steady-state values are less negative for cases with higher permeability, underscoring the influence of permeability on the rate and

magnitude of pore-water pressure dissipation throughout the consolidation process. These findings emphasize the critical role of soil permeability in determining the short-term and long-term responses following excavation activities.

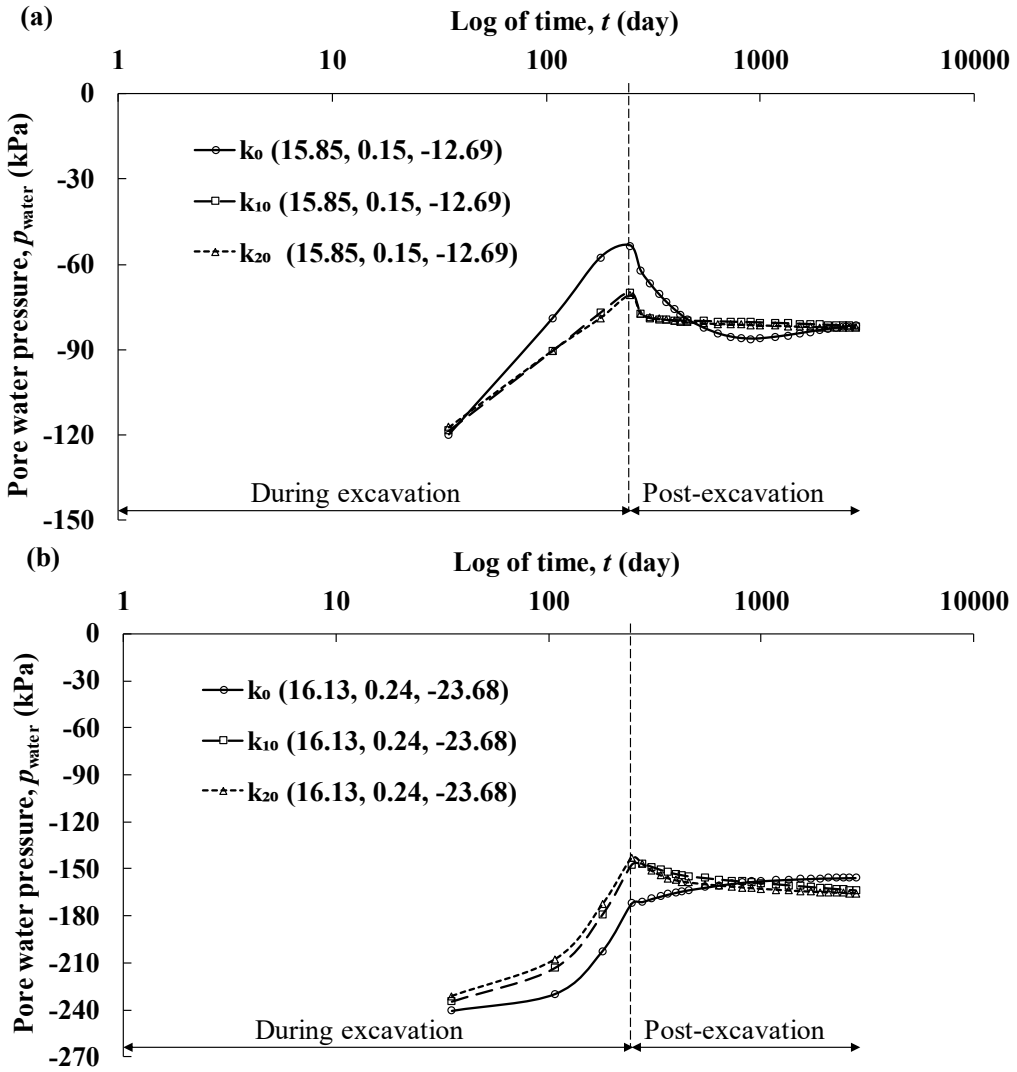

Figure 12: Effect of soil permeability on active pore-water pressure (p_{water})

4. CONCLUSIONS

This study employed the HS-small soil model to perform a three-dimensional time-dependent analysis of deep excavation in clayey soil subjected to an adjacent surcharge. The excavation, 15 m deep and 30 m wide, was supported by a three-level anchored diaphragm wall system. The analysis examined the effects of excavation length and soil permeability on key response parameters, including the maximum wall displacement (u_{max}), maximum bottom heave ($u_{z,max}$) and pore-water pressure distribution. The major findings of the study are as follows:

1. During excavation, wall displacements for L/B ratios of 3 and 2 remain closely aligned up to the third excavation stage, while the L/B = 1 case consistently shows smaller values. The variation among all cases becomes negligible during the post-excavation period. All models exhibit similar heave behavior; however, post-excavation results indicate greater bottom heave for a lower L/B ratio. The excess pore-water pressure response for L/B ratios of 3 and 2 follows similar trends, whereas L/B = 1 maintains lower values throughout both phases. Although pore-water pressure

decreases uniformly during excavation across all cases, post-excavation behavior diverges, with lower L/B ratios showing a higher increase in compressive stresses.

2. Wall displacement and bottom heave progressively increase with higher soil permeability during the excavation phases. After excavation, wall displacement tends to stabilize, whereas bottom heave continues to increase as permeability increases. During excavation, soil with higher permeability exhibits a reduced generation of excess pore-water pressure. Post-excavation, such soils exhibit a slower rate of dissipation of excess pore-water pressure. Consequently, soils with higher permeability (k_{10} and k_{20}) follow similar trends but experience a smaller overall reduction in p_{water} compared to the base case (k_0). Over an extended time, pore pressure attains a stable state with final values being less negative in soils exhibiting higher permeability.

ACKNOWLEDGEMENTS

The authors acknowledge the Department of Civil Engineering, IIT Guwahati, Assam, India, for providing the necessary computing facilities.

DECLARATION OF USE OF AI

The authors declare that AI tools were used solely for language editing and grammar correction to improve sentence flow, and no AI-generated content or analysis was included in the research or results.

REFERENCES

Briaud, J. L., & Lim, Y. (1999). Tieback walls in sand: numerical simulation and design implications. *Journal of Geotechnical and Geoenvironmental Engineering*, *125*(2), 101–110.

Brinkgreve, R., Swolfs, W., & Engin, E. (2015). PLAXIS user's manual, version 6.1. Balkema, Rotterdam, The Netherlands.

Calvello, M., & Finno, R. J. (2004). Selecting parameters to optimize in model calibration by inverse analysis. *Computers and Geotechnics*, *31*(5), 410–424.

Clough, G. W., & O'Rourke, T. D. (1990). "Construction induced movements of in situ walls". Proc., ASCE Conf. on Des. and Perf. of Earth Retaining Struct., Geotech. Spec. Publ. No. 25, ASCE, New York, 439–470.

Finno, R. J., & Roboski, J. F. (2005). Three-dimensional responses of a tied-back excavation through clay. *Journal of Geotechnical and Geoenvironmental Engineering*, *131*(3), 273–282.

Finno, R. J., Blackburn, J. T., & Roboski, J. F. (2007). Three-dimensional effects for supported excavations in clay. *Journal of Geotechnical and Geoenvironmental Engineering*, *133*(1), 30–36.

Harahap, S. E., & Ou, C. Y. (2020). Finite element analysis of time-dependent behavior in deep excavations. *Computers and Geotechnics*, *119*, 103300.

Hejazi, Y., Dias, D., & Kastner, R. (2008). Impact of constitutive models on the numerical analysis of underground constructions. *Acta Geotechnica*, *3*(4), 251–258.

Hsiung, B. C. B., Yang, K. H., Aila, W., & Ge, L. (2018). Evaluation of the wall deflections of a deep excavation in Central Jakarta using three-dimensional modeling. *Tunnelling and Underground Space Technology*, *72*, 84–96.

Long, M. (2001). Database for retaining wall and ground movements due to deep excavations. *Journal of Geotechnical and Geoenvironmental Engineering*, *127*(3), 203–224.

Lu, T., Wu, K., Liu, S., & Cai, G. (2023). Method for estimating three-dimensional effects on braced excavation in clay. *Tunnelling and Underground Space Technology*, *141*, 105355.

Ou, C. Y. (2006). *Deep excavation: Theory and practice* (1st ed.). Taylor & Francis, London.

Sabatini, P. J., Pass, D. G., & Bachus, R. C. (1999). *Ground anchors and anchored systems* (No. FHWA-IF-99-015). United States. Federal Highway Administration. Office of Bridge Technology.

Schanz, T., Vermeer, P. A., & Bonnier, P. G. (1999). *The hardening soil model: Formulation and verification*. In Beyond 2000 in computational geotechnics (pp. 281–296). Routledge.

Sills, G. C., Burland, J. B. & Czechowski, M. K. (1978). "Behaviour of an anchored diaphragm wall in stiff clay". Proc. Ninth Int. Conf. Soil Mech. Fdn. Engg., Tokyo, 2**,** 147−155.